Progress in Natural Science: Materials International 26 (2016) 347–353

HOSTED BY

Contents lists available at ScienceDirect

Progress in Natural Science: Materials International

journal homepage: www.elsevier.com/locate/pnsmi

Original Research

Crystal and electronic structure study of Mn doped wurtzite ZnO nanoparticles

O.M. Ozkendir [a,b,*], S. Yildirimcan [b,c], A. Yuzer [b], K. Ocakoglu [a,b]

[a] Department of Energy Systems Engineering, Mersin University, Tarsus Faculty of Technology, 33480 Mersin, Turkey
[b] Advanced Technology Research & Application Center, Mersin University, Ciftlikkoy Campus, Yenisehir, Mersin, Turkey
[c] Faculty of Engineering, Department of Electrical-Electronics Engineering, Toros University, TR-33140 Mersin, Turkey

ARTICLE INFO

Article history:
Received 6 January 2016
Received in revised form
13 July 2016
Accepted 29 July 2016
Available online 10 August 2016

Keywords:
Electronic materials
Nanostructures
Oxides
XAFS (EXAFS and XANES)
Crystal structure

ABSTRACT

The change in the crystal and electronic structure properties of wurtzite ZnO nanoparticles was studied according to Mn doping in the powder samples. The investigations were conducted by X-ray Absorption Fine Structure Spectroscopy (XAFS) technique for the samples prepared with different heating and doping processes. Electronic analysis was carried out by the collected data from the X-ray Absorption Near-Edge Structure Spectroscopy (XANES) measurements. Additional crystal structure properties were studied by Extended-XAFS (EXAFS) analysis. Longer heating periods for the undoped wurtzite ZnO samples were determined to own stable crystal geometries. However, for some doped samples, the distortions in the crystal were observed as a result of the low doping amounts of Mn which was treated as an impurity. Besides, the changes in oxygen locations were determined to create defects and distortions in the samples.

1. Introduction

ZnO is a member of II–VI compound semiconductors group with a wide bandgap property. ZnO compounds mainly form in two different crystal structures, i.e., hexagonal wurtzite and zinc blende. The hexagonal wurtzite structure is the most studied ZnO crystal because of its potential to emerge surprising properties due to the asymmetry in the crystal geometry. Although the electronic and optical properties ZnO have been studied intensively, it is still one of the most popular subjects in current studies and attracting great interest due to high applicability in current technology, such as high transparency, luminescence at room-temperature or high mobility, etc. [1]. Additionally, the nanostructure forms (nanowires and nanorods) of ZnO have various novel properties that make them most desired materials due to the high performance in the solar cells or electronic devices, such as Schottky diode [2,3]. Synthesis of nanostructured materials is important to use the novel properties of materials in technological applications [4,5].

Like the ZnO nano compounds, doped ZnO samples also find place in the family of transparent conducting oxides with an important amount of potential in technological applications, like thermal coatings for windows, spintronic devices and solar cells etc. [6]. However, there is still a lack of investigation to understand the influence of doping which may emerge surprising electronic properties. On the other hand, doping can cause defects in the structure. Defects treated as imperfection of the crystals but sometimes they may reveal fruitful electronic or crystal properties. The role of defects in ZnO oxides and their influence on both electronic and magnetic behaviors were recently reported by Shashi et al. [7]. Their study was mainly focused on the background of d^0 magnetism in nanostructured ZnO materials and the influence of defects by XANES technique.

In this study, the crystal and electronic structure properties of the Mn doped wurtzite ZnO compounds were examined by X-ray Absorption Fine Structure Spectroscopy (XAFS) technique. Additionally, influences of the doping on the electronic properties of both Zn and O atoms were probed. To study the crystal and electronic properties of materials, XAFS is a useful method and it can be separated into two sections as XANES and EXAFS (Extended-XAFS). The XANES part of the XAFS technique contains the information about the electronic structure of the interested atom in the material and allows us to determine the local electronic arrangement of atoms. The EXAFS part lies 40–50 eV above the main absorption edges of atoms. The interference of the outgoing photoelectron wave and the tails of this wave backscattered from the neighboring atoms yield EXAFS data. EXAFS technique has a great interest because of the possibility to extract the information from the periodicity of the oscillations in the EXAFS region. This allows us to estimate the bond lengths, the amplitudes of the fine structure and provides information about the number of atoms that surround the absorbing atom [8,9].

* Corresponding author at: Department of Energy Systems Engineering, Mersin University, Tarsus Faculty of Technology, 33480 Mersin, Turkey.
E-mail address: ozkendir@gmail.com (O.M. Ozkendir).
Peer review under responsibility of Chinese Materials Research Society.

http://dx.doi.org/10.1016/j.pnsc.2016.07.004

To achieve better results for the analysis, XAFS measurements were supported by the performed Zn K-edge calculations with FEFF 8.2 code [10]. In the calculations, Hedin-Lundqvist exchange correlation potential was used and a FEFF input file was created by the ATOMS package. The full multiple scattering calculations for one nanometer thick ZnO cluster containing 340 atoms (Zn, O) were performed. In the prepared input file for the calculations, a Zn atom in the wurtzite ZnO cluster was selected as the absorber and a photoelectron emitter. For such a sample, the number of the atoms and the thickness are so less. However, the calculation process mainly depends on the electronic transitions in coordination with the bonding of the absorbing atom with its nearest neighbors. So, it is possible to obtain highly accurate data with small amount of atoms. In the calculations, the backscattering and phase shifts with single and multiple scattering paths were calculated for Extended-XAFS (EXAFS) spectra at the temperature of 70 °C.

2. Experimental

Zinc oxide samples were prepared at Advanced Materials Research Center (MEITAM) laboratories of Mersin University with different procedures of preparation steps. The samples were prepared by dissolving of $Zn(NO_3)_2 \cdot 6H_2O$ (2.97 g) in 100 ml distilled water, and then the addition of PEG300 (3.36 g). Afterwards, pH of the each solution adjusted to 10 by the addition of NH_3. With different time periods, the samples were prepared at autoclave at 70 °C, filtered and dried at 80 °C. The preparation time periods for the samples at autoclave were 1 h, 6 h, 12 h, 24 h and 36 h. For a better interpretation in the analysis, these samples were coded as S_{27} (1 h), S_{28} (6 h), S_{29} (12 h), S_{30} (24 h) and S_{31} (36 h). Besides, the sample with the synthesized time of 6 h also doped with different amounts of manganese by adding different molar concentration of $Mn(NO_3)_2 \cdot 4H_2O$. The molar concentrations in the samples are 0.001% Mn^{2+}, 0.01% Mn^{2+}, 0.05% Mn^{2+}, 0.1% Mn^{2+}, 0.25% Mn^{2+}, 0.75% Mn^{2+}, 1% Mn^{2+}, 2.5% Mn^{2+}. For ease, the doped samples are coded as S_{41}, S_{42}, S_{43}, S_{44}, S_{45}, S_{46}, S_{47} and S_{48}, respectively. The doped and undoped ZnO nanopowders were prepared according to the reported method in literature [11]. The SEM images of the samples are given in Fig. 1(a) and (b). SEM image (a) was taken from an undoped sample and (b) was taken from a Mn-doped sample. The nanoparticle shapes are determined as 1–7 μm long nanorods with a diameter of 100–200 nm. Besides, to support the morphological data of the Mn doped nano ZnO particles, TEM images of samples are given in Fig. 2 and related EDX graph is given in Fig. 3. The EDX results of the sample analysis are given in Table 1.

The morphological properties can be well studied by XRD patterns. To show the disturbance in ZnO to Mn doping even with so small amount, the XRD pattern for the sample S_{41} (0.001% Mn^{2+}) is given in Fig. 4. Mn presence in the crystal shows itself with tiny peaks at 20° and 27° on 2Θ scale which does not exist in pure ZnO nanoparticle XRD patterns as reported in the previous literature [12]. The highest intensity on the XRD pattern was determined from the (101) layer and confirms the wurtzite crystal structure. The second and the third highest reflection peaks were determined from the layers (100) and (002), respectively. Influence of Mn doping on the electronic properties of wurtzite ZnO nanostructures were probed by XANES measurements.

To probe the electronic properties of the samples, XANES data were collected by the performed measurements at MAX-Lab synchrotron radiation facility of Lund University in Lund (Sweden). Zn and Mn $L_{3,2}$-edge and O K-edge XANES data were collected at the beamline I1011 on MAX-Lab in TEY (Total Electron Yield) mode, at room temperature and under ultra high vacuum (UHV) ($\sim 10^{-10}$ Torr) conditions. The beamline I1011 is located on the ring MAX-II, using an elliptically polarizing undulator and providing soft x-ray with a variable polarization state [13].

To support the XANES study the complementary XAFS measurements of the samples for Zn K-edge were performed at beamline BL8: XAS on Siam Photon (SLRI) Synchrotron Radiation facility in Nakhon Ratschasima (Thailand) [14,15]. XAFS data were collected in transmission mode at room temperature. The measurements were supported by XAFS calculations by using the commercial FEFF 8.2 code [16]. In the calculations, FEFF input files generated by the ATOMS software with lattice parameters of ZnO for wurtzite structure as given in the literature [17]. Besides, for further crystallographic analysis, the backscattering and phase shift with single and multiple scattering paths were calculated to obtain the EXAFS spectra. According to the measurements, the lattice parameters were defined as $a=0.324$ nm, $b=0.324$ nm and $c=0.520$ nm with support of the calculations.

3. Results and discussion

For the 3*d* transition metals, XANES L-edge spectra are so sensitive to the interactions with the neighboring atoms and the chemical states of atoms, where the transition of 2*p* electrons to the empty levels over the Fermi level as a final state takes place. In Fig. 5, Zn L_3 and L_2 edge XANES spectra of undoped ZnO nanorod

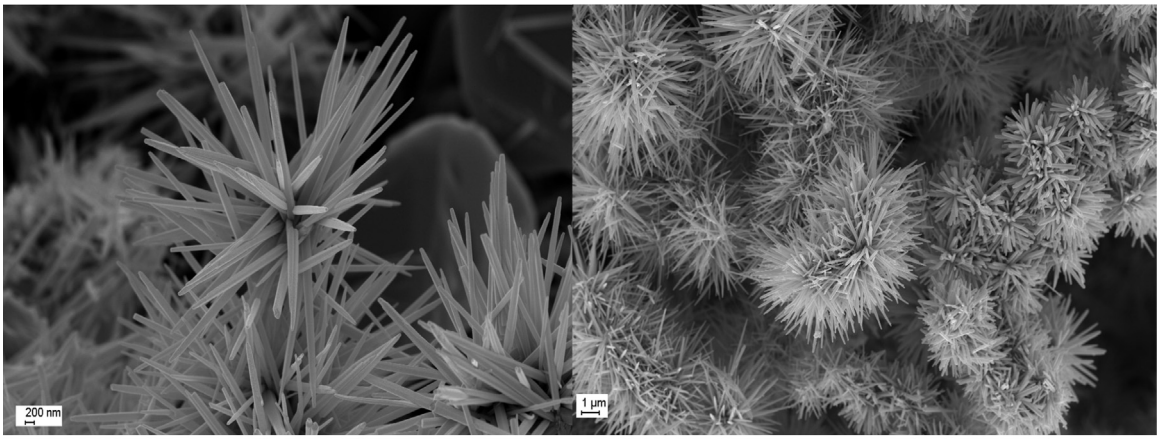

Fig. 1. SEM images from the nano ZnO samples: (a) undoped sample and (b) Mn-doped sample.

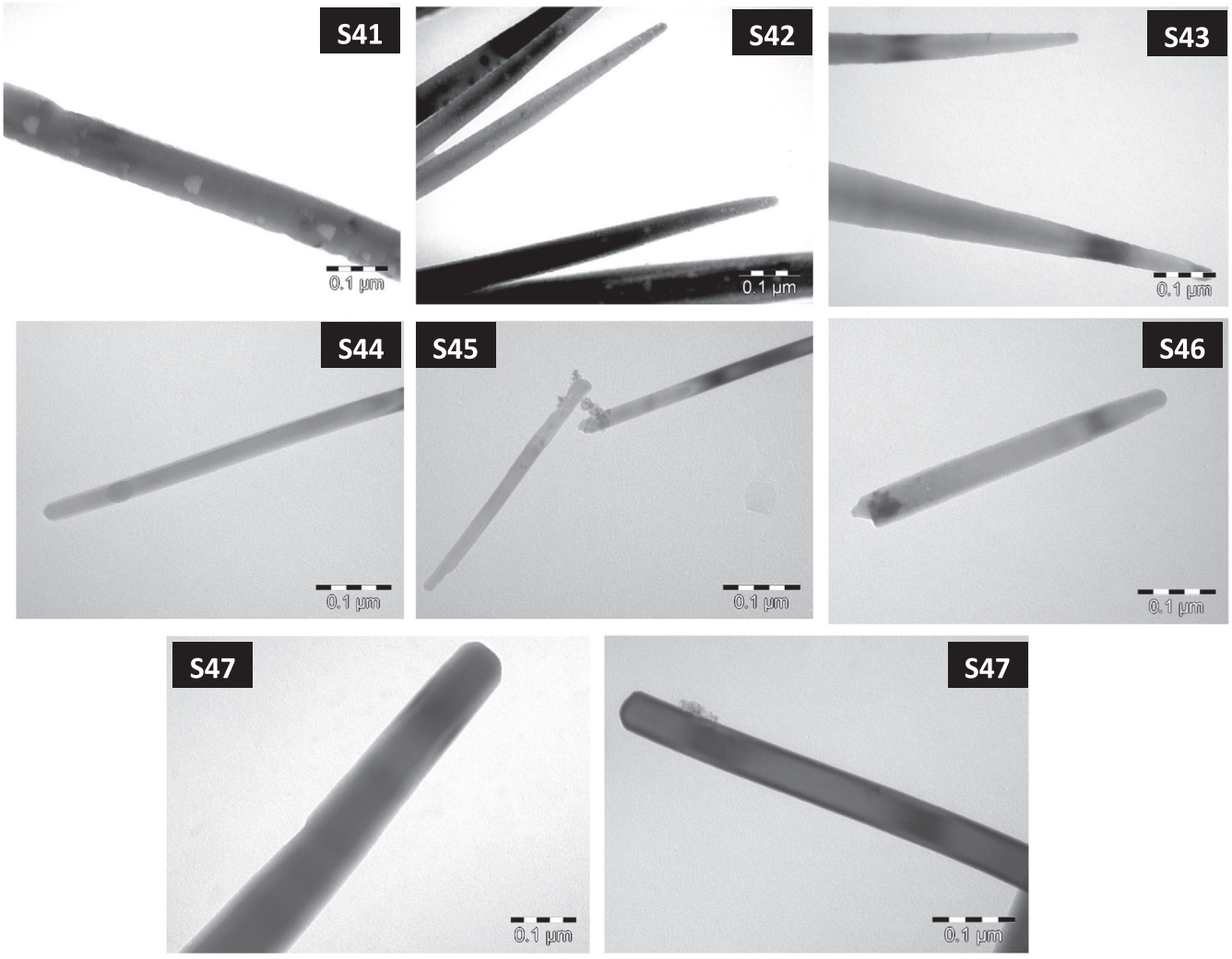

Fig. 2. TEM images for the Mn doped samples.

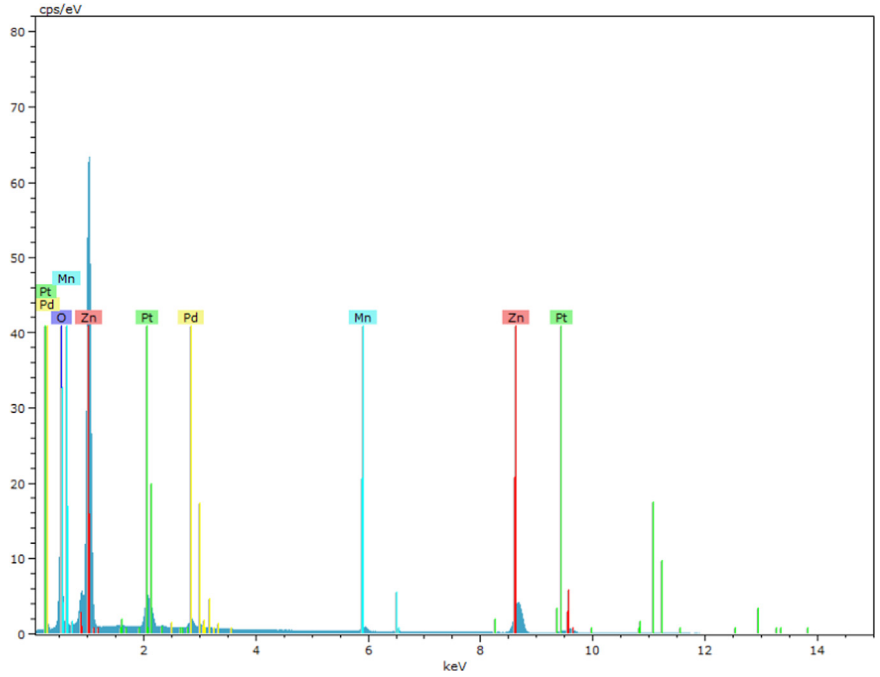

Fig. 3. EDX results for the Mn doped ZnO samples.

Table 1
EDX analysis results of the Mn doped wurtzite ZnO samples.

El AN	Series	Unn. [wt%]	C norm. [wt%]	C atom [at%]	C error (1 Sigma) [wt%]
Zn 30	K-series	65.46	66.27	41.89	2.19
O 8	K-series	20.64	20.89	53.97	2.38
Pt 78	M-series	8.65	8.75	1.85	0.36
Pd 46	L-series	2.13	2.16	0.84	0.10
Mn 25	K-series	1.91	1.93	1.45	0.09

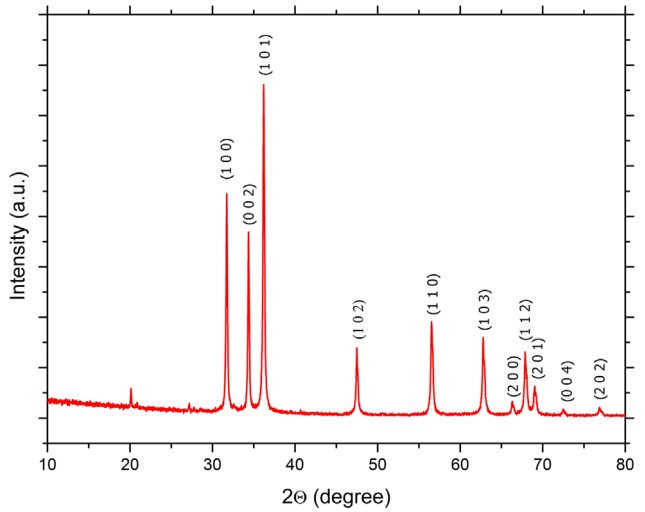

Fig. 4. XRD pattern of the sample S_{41} (0.001% Mn^{2+}). The Mn presence appeared with tiny peaks at 20° and 27°.

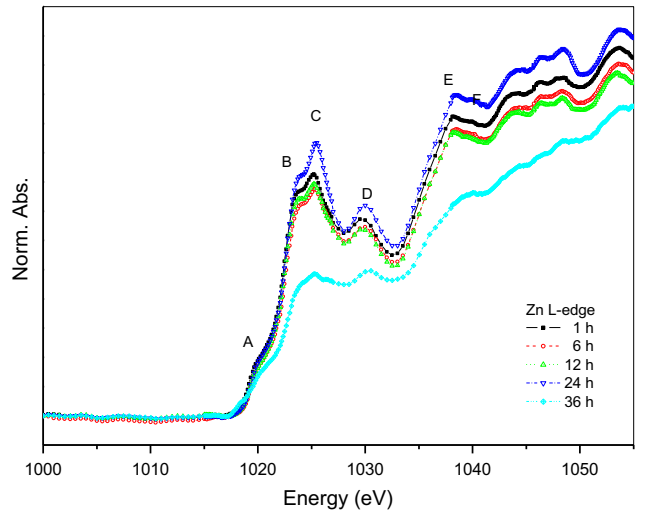

Fig. 5. Compared XANES spectra of Zn $L_{3,2}$-edges due to preparation process periods.

samples are given. The origin of separated spectra of the L-edge ($L_{3,2}$-edges) are the spin-orbit interaction of the 2*p* core electrons with the holes of the valence levels where they sit as a final state. Mainly, the Zn $L_{3,2}$ edge absorption peaks correspond to the transition of $2p_{3/2,1/2}$ core electrons to the unoccupied 4*d* levels as final states. The Zn L_3 edge absorption spectrum has four maxima which is assigned as A, B, C and D. The spectrum begins to rise at 1017 eV and have maxima for the assigned peaks at photon energies as 1020 eV, 1023.4 eV, 1025.5 eV and 1029.8 eV, respectively. Beyond the L_3 edge, Zn L_2 absorption edge assigned as "E" lies and has a main absorption peak at 1038 eV. The multipeak structure of $L_{3,2}$-edge spectra of Zn is a result of its crystal structure which provides more convenient quantum symmetries for the excited electrons to occupy as a final state and to construct larger molecular orbitals via strongly overlapped wave functions and mixing of 3*d*-4*p* levels.

For analysis, the XANES region can be studied in three regimes as the "pre-edge", "main-edge" and the "post-edge". The peak "A" is called as pre-edge and provides information both about the forbidden electron transitions, which does not obey dipole selection rules and disorder in the crystal geometry. The pre-edge feature appears at the low energy level and appears because of the asymmetry in the wurtzite structure, and *p* electrons transition to *d* or *p* level obeys the dipole selection rules. The "B" and "C" main absorption edge peaks are related to the transition of 2*p* electrons to the Zn 4*p* levels as final states. The intensities of the absorption peaks are related to the available unoccupied states for the excited electrons. The higher intensities reflect the transition to almost unoccupied *p* levels. Beyond the peak "C", a shoulder like peak "D" at 1029.8 eV is located. It corresponds to the high energy levels on the molecular band and occurs as a result of weaker *d*-*d* interaction between the source and neighboring Zn 4*d* levels.

Sharp absorption peak intensities of the samples refer to the sensitivity of the electron transitions from 2*p* levels to the unoccupied 3*d* or 4*p* levels. However, for bulk ZnO samples, the peak intensities are expected to have larger and Gaussian shape with higher intensities due to the contribution from more atoms [18]. According to the collected Zn $L_{3,2}$-edge XANES spectra of ZnO samples, it confirms that the increasing time periods enrich the zinc purity in the solutions by forming more stable crystalline structure. The tiny decrease in the peak intensities of the 6 h heated sample is a result of the reduced overlapping between neighboring atoms due to atomic oscillations. Beyond 6 h period, the intensities increased and the highest intensity reached at the sample with 24 h preparation process which means stronger coupling and overlapped outer shell electrons of the neighboring atoms and Zn. By heating the sample, stronger bonds established while weaker bonds ruined. Despite the different peak intensities, all the samples preserve their symmetries, i.e., no distortions in the electronic interplay. As mentioned above, the intensity of the absorption peaks are related to the unoccupied states over the Fermi level. Thus, it can be concluded with the increasing absorption edge that stronger overlapping construct broader molecular bands with more unoccupied states on the neighboring outer shell levels of the atoms. However, beyond 24 h period, i.e., 36 h period, decrease in the intensity of the Zn L-edge is clear. Besides, existence of a tiny pre-edge structure reflects a distorted crystal structure formation with weakly interacting neighboring levels and may cause defects in the structure.

Mn doped ZnO samples with a similar preparation process of the sample S_{28} were encoded as S_{42}–S_{48}. In Fig. 6, XANES spectra of the Zn $L_{3,2}$-edge of Mn doped samples are given in comparison to determine the effects of doping on the electronic structure of Zn and its environment. The spectral intensities of the samples have higher absorption intensities except the samples $S_{42–43}$ with the small doping amount of Mn. The spectra of the samples $S_{42–43}$ are noisy and have weaker intensity. The spectral feature of the samples $S_{42–43}$ with lower Mn concentration is reflecting an impurity in the structure which may be caused as a result of local defects due to imbalanced atomic ratios. However, for the samples S_{44}–S_{48}, collected data for Zn $L_{3,2}$-edge yield better spectra with an increasing intensity where all peaks are in symmetry. The increase in the intensities is parallel to the increase in Mn concentration in the bulk and highlights the construction of stable crystal structure with overlapped molecular bonds.

To make the dopant effects in the crystal more clear, Mn $L_{3,2}$-edge structure are also given in Fig. 7 as an image from the dopants' side. Mn $L_{3,2}$-edge spectra are given in comparison of the

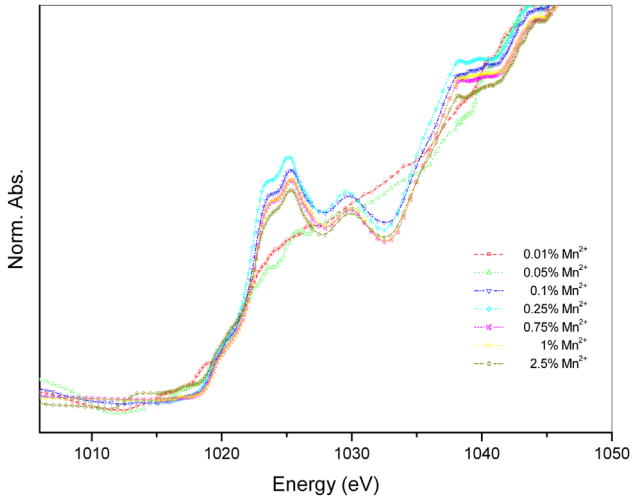

Fig. 6. To figure out the effects of the Mn doping process on the electronic structure of the wurtzite ZnO, the spectral change comparison is given via XANES Zn $L_{3,2}$-edge spectra.

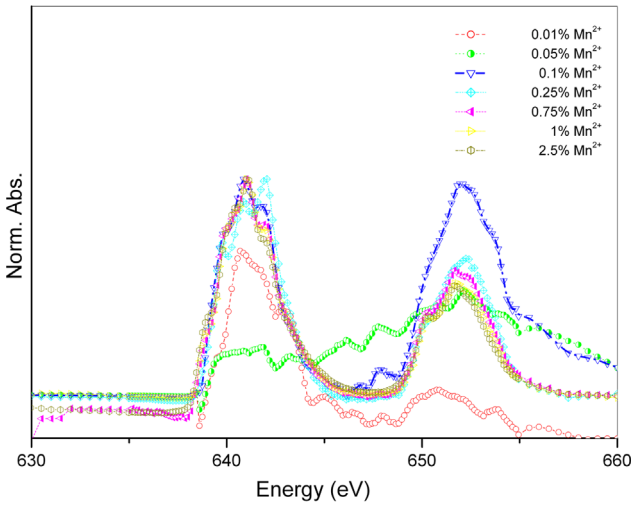

Fig. 7. Comparison of the Mn $L_{3,2}$-edge XANES spectra to provide a view about the electronic structure change due to Mn doping from the Mn side.

doped samples, i.e. $S_{42–48}$. L_3-edge XANES spectra of Mn atoms have multiplet feature like in the Zn L_3-edge spectrum. Besides, similar noisy and vague spectral features for samples $S_{42–43}$ presented in the figure and confirms the corruption in the samples due to lower Mn doping. In other words, low amount of doped Mn atoms behave like an impurity and cause distortion in the wurtzite ZnO crystal structures. For the samples with higher Mn concentrations than S_{43}, more stable crystal formation was observed with smoother absorption spectra. The phenomena emphasizes an evidence that Zn atoms preserve their locations and geometry and doped Mn atoms were integrated with the local Zn and O atoms in the crystal, for minimum doping rate of 0.25% and beyond.

Mn $L_{3,2}$-edges are due to the $2p_{3/2,1/2}$ excited electrons' transitions to the unoccupied $2p \rightarrow 2p^6 3d^5$ ground state or $2p \rightarrow 2p^5 3d^6$ mixed (excited state) levels. 3*d* levels of the transition metals (TM) have five-fold degeneracy with low energy (t_{2g}) and high energy (e_g) levels to neighboring atoms during bonding. The degeneracy of the 3*d* levels provides rich oxidation states when TM's oxidized. The low energy peaks (t_{2g}) occurred via O2*p*-Mn3*d* hybridizations which are overlapped by neighboring Zn 4*d* levels. The L_3 main edge has a maximum at 641 eV. Beyond the main edge, a small shoulder like e_g peak appears due to the interaction between Zn

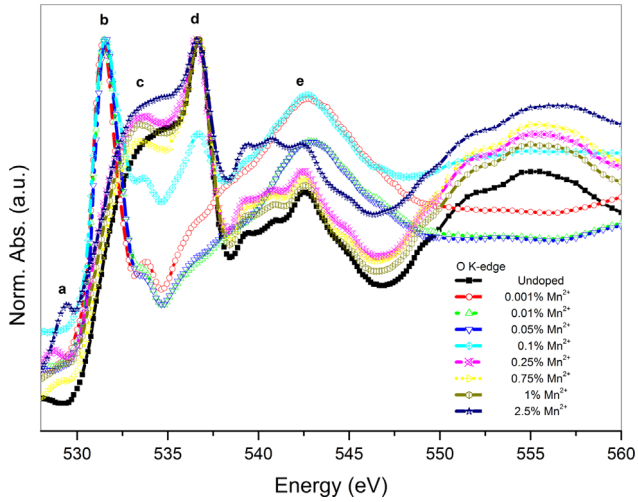

Fig. 8. The compared O K-edge XANES spectra in Mn doped samples with undoped ZnO sample S_{28}.

4*p* and Mn 3*d* levels. The L_2-edge has two maxima at energies of 650.3 eV and 651.7 eV, respectively. The multiple structure of the L_2-edge spectra, like L_3-edge, appears as a result of five-fold degeneracy in the *d*-levels.

To obtain a broader perspective for the analysis, O K-edge XANES in the wurtzite ZnO structures are given in Fig. 8 for the doped samples. In oxides, oxygen atom has a key role and provides rich symmetries to its neighbors. Moreover, they can build strongly overlapped molecular bonds with all other members of the materials and they link metals to each other. Also, oxygen is the most popular agent for analysis because of being so sensitive to the local bonding and symmetry. The O K-edge XANES spectra of the samples S_{42}, S_{43} and S_{44} have pre-edge with two peaks, assigned as "b" and "c" with maxima of 533.52 eV and 536.6 eV, respectively. S_{44} sample spectra have similar peak intensities both like S_{42-43} and $S_{45–48}$ samples. The spectra highlight the change in the electronic interactions of oxygen and its neighbors. The samples S_{28} and S_{47} have also two peak pre-edge structure in symmetry with the assigned peaks "b" and "c", but the samples S_{45}, S_{46}, S_{47} and S_{48} have an extra pre-edge peak "a" reflecting the Mn contribution to bonding.

The sharp intensity of the pre-edge structure is a result of both the asymmetry of the wurtzite structure and the forbidden electron transition due to the atomic selection rules in the electric dipole approximation; i.e. $1s \rightarrow 3d/4p$. The existence of the two peaks at the pre-edge confirms the presence of low (t_{2g}) and high energy (e_g) levels [9]. Besides, as a result of five-fold degeneracy of Mn 3*d* levels, they can provide strongly overlapped broad *p-d* hybrid molecular bands which are rich in quantum symmetries. The pre-edge peaks "a", "b", "c" and "d" are both due to the transitions from O 1*s* to O2*p*-[Zn 4(*p*), Mn 3*d*] hybridized levels. The peak "b" disappeared in the smooth ZnO and ZnO:Mn samples spectra and the pre-edge became a lower energy part of the main edge. This spectral feature exists with the increasing Mn concentrations starting from the 0.1% Mn doped samples and confirms Mn contribution to the construction of the broader molecular bands via strongly overlapped levels. The increase in the "c" and "d" peak intensities of the sample S_{44} confirms localization of Mn atoms in the ZnO. Beyond the pre-edge, the main edge peak is located with a maximum of 542.68 eV and assigned as "e". The main edge peak is due to the O 1*s* core electrons transition to O 2*p* levels. To obtain the background information to reveal the change in the electronic properties of oxygen, EXAFS analysis can provide more powerful tools for analysis. For this purpose and to clarify

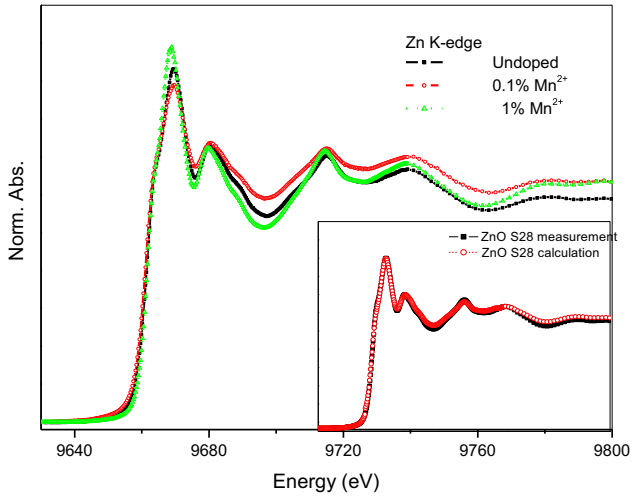

Fig. 9. Comparison of the XANES measured spectra of Zn K-edge with undoped, 0.1% Mn^{2+}, 1% Mn^{2+} (i.e., S_{28}, S_{44} and S_{47}) samples . Inset, the agreement between measurement and the calculation for undoped sample.

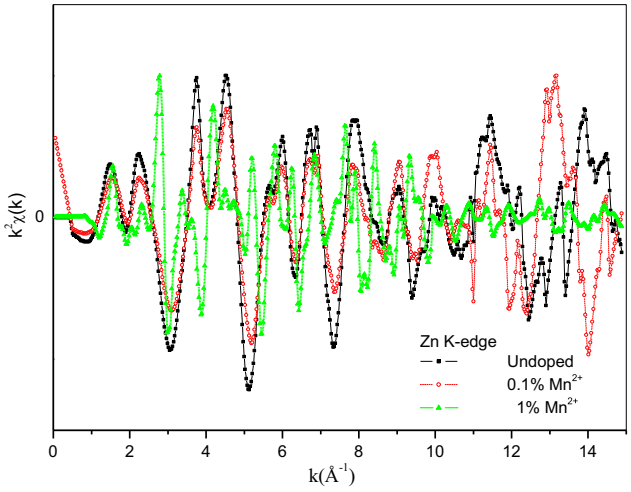

Fig. 10. Compared EXAFS Chi signal of the samples S_{28}, S_{44} and S_{47}.

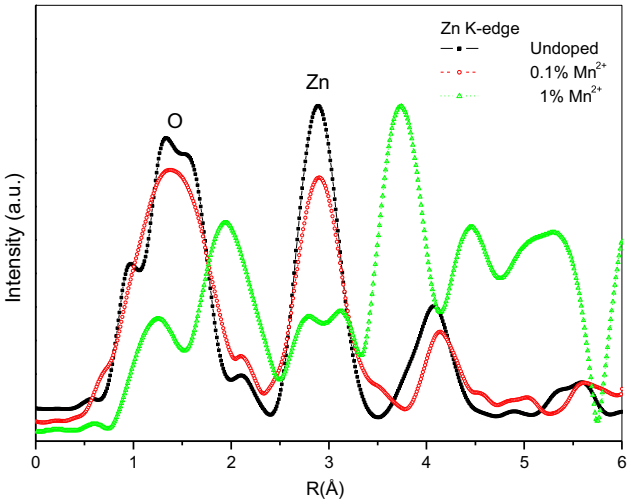

Fig. 11. Compared RDF peaks for the samples S_{28}, S_{44} and S_{47}.

the crystal of the samples, XAFS measurements were performed at SLRI BL: XAS and supported by the FEFF calculations.

In Fig. 9, Zn K-edge spectra of S_{28}, S_{44} and S_{47} samples are compared to reveal the structural disorder stated in the $L_{3,2}$-edge analysis. The comparison of the measured Zn K-edge XAFS spectra are given in the inset of the figure with the FEFF calculation. The calculated Zn K-edge spectra have a significantly high agreement with the measured spectra and provide useful tools that can guide for analysis.

The K-edge absorption peak of Zn is due to the transition of 1*s* core electrons' to the unoccupied 4*p* levels as a final state. The absorption edge begins to rise at 9651.5 eV and have a maximum at 9670 eV. Below the main edge, a weak edge at 9663 eV appeared and it is obviously due to the asymmetry of the wurtzite bonds since the 3*d* levels are fully occupied in Zn atoms. In the spectra, the peaks also seem to keep their symmetry, however K-edge spectra of the sample S_{47} has a slight shift on the main edge which can be a sign of change in the Zn-O bonding. The slight shift implies ionic Zn atoms due to electron share during bonding interactions. The EXAFS study is a good choice for better crystal analysis. The data for the EXAFS analysis can be extracted from the measured XAFS spectra by using ATHENA and ARTEMIS software [18]. The analysis on the crystal structure of the samples would be carried out by ARTEMIS software with the generated paths from FEFF calculations by making fits.

In Fig. 10, the EXAFS "chi" (χ) intensity is given for the corresponding wave number (k). In the "low" k values, the S_{28} and S_{44} samples have a high agreement in symmetries. However, for sample S_{44}, the weak decrease in intensity and distortion in symmetry at higher k values mean increasing disorder with the increasing molar concentration of the dopants. The chi signal of the sample S_{47} has a sharp decay at higher k values and almost out of symmetry. The answer to the question of "What happened in the bulk? " can be found in the Radial Distribution Function (RDF) of the EXAFS chi data. The compared RDF data of S_{28}, S_{44} and S_{47} samples are given in Fig. 11. The peaks are labeled with "mainly" consisted atomic symbols.

The S_{28} sample owns wurtzite structure which has asymmetric O bond lengths with Zn atoms as (Zn-O): 0.1794 nm and 0.2034 nm. This difference in the near neighboring atom distances is the origin of the asymmetry in the wurtzite structure. To determine the exact atomic locations and types, FEFF calculation fits for wurtzite ZnO cluster were performed. In Table 2, fitted atomic locations of the undoped Sample S_{28} are given for wurtzite ZnO in one direction with 0.4 nm distance. According to Fig. 10, all oxygen locations have shifted to distant locations in the atomic coordination from the source Zn atom. Although Zn atoms keep their locations, shift in the O coordination obviously seen both for the samples S_{44} and S_{47} as an evidence for reorganization according to the doped Mn atoms. Mn atoms bond with oxygen atoms and mainly tend to construct isolated structures like MnO or MnO_2; i.e., salt halide, cassarite or orthorhombic.

Table 2
Fitted RDF results of atomic locations for undoped wurtzite ZnO sample.

Compound	Source atom	Type of atom	*R* (nm)[a]
ZnO	Zn	O	0.1794
		O	0.2037
		Zn	0.3200
		Zn	0.3240
		O	0.3406
		O	0.3704
		O	0.3827
		O	0.3831
		O	0.4074
		Zn	0.4056
		O	0.4701

[a] Inter-atomic distances (± 0.002 nm).

4. Conclusions

The crystal and electronic properties of undoped and Mn doped wurtzite ZnO nanoparticles were studied by XAFS technique for the samples with different heating and doping preparation processes. Longer heating periods for the undoped wurtzite ZnO were determined to build more stable crystal structures. However, for Mn doped samples with small doping ratio, the distortions in the crystal were observed as a result of the low doping concentration of Mn and treated as impurity in the samples. For the samples with higher Mn concentrations than in the sample S_{43}, more stable crystal formations were observed. The main reason for the distortions is determined as a result of the changes in the oxygen locations. Besides, the symmetry for the highly doped samples was observed in the absorption spectra highlighting stable Zn atoms that preserve their locations in the wurtzite geometry.

Also, O K-edge XANES spectra of the samples provide us the traces of the change in the electronic interactions of oxygen atoms with its neighbors. The sharp intensity of the pre-edge structure of O K-edge were determined to refer the forbidden electron transitions due to the dipole selection rules in the electric dipole approximation, i.e. $1s \rightarrow 3d$ and the asymmetry in the nature of the wurtzite structure. With the S_{28} sample spectra, the asymmetric O bond lengths with Zn atoms can be estimated as 0.1794 nm and 0.2034 nm. Besides, the EXAFS studies reveal the disturbance in the crystal structure where Mn atoms mainly tend to construct isolated structures like MnO or MnO_2.

Acknowledgement

The authors would like to thank Dr. Gunnar Ohrwall from MAX-Lab., Dr. Wantana Klyusubun and her staff from SLRI (Siam Photon) for their technical support and great hospitality.

S. Yildirimcan and K. Ocakoglu thank The Scientific and Technological Research Council of Turkey (TUBITAK) (Grant: 110M803) for financial support.

This study is partly supported financially by “BAP-TTEF EEEME (OMÖ) 2012–7” project of Mersin University (Mersin, Turkey).

The research leading to these results has received funding from the European Community's Seventh Framework Program (FP7/2007–2013) CALIPSO under Grant agreement no. 312284.

References

[1] U. Ozgur, Ya.I. Alivov, C. Liu, A. Teke, A.M. Reshchikov, S. Doğan, V. Avrutin, S.-J. Cho, H. Morkoc, J. Appl. Phys. 98 (4) (2005) 041301.
[2] P. Tiwari, H. Srivastava, A.K. Srivastava, S.K. Deb, J. Alloy. Compd. 611 (2014) 111–124, http://dx.doi.org/10.1016/j.jallcom.2014.05.057.
[3] G.-H. Nam, S.-H. Seong-Ho Baek, I.-K. Park, J. Alloy. Compd. 613 (2014) 37–41, http://dx.doi.org/10.1016/j.jallcom.2014.05.110.
[4] C. Wei, C. Cheng, B. Zhou, X. Yuan, T. Cui, S. Wang, M. Zheng, H. Pang, Part. Part. Syst. Charact. 32 (2015) 831–839, http://dx.doi.org/10.1002/ppsc.201500018.
[5] C. Wei, C. Cheng, S. Wang, Y. Xu, J. Wang, H. Pang, Chem. Asian J. 10 (2015) 1731–1737, http://dx.doi.org/10.1002/asia.201500335.
[6] T. Hanada, Oxide and nitride semiconductors, in: T. Yao, S.-K. Hong (Eds.), Advances in Materials Research, vol. 12, Springer, Berlin, Heidelberg, 2009, pp. 1–19.
[7] B.S. Shashi, Y.F. Wang, Y.C. Shao, H.Y. Lai, S.H. Hsieh, M.V. Limaye, C.-H. Chuang, H.C. Hsueh, H. Wang, J.W. Chiou, H.M. Tsai, C.W. Pao, C.H. Chen, H.J. Lin, J.F. Lee, C.T. Wu, J.J. Wu, W.F. Pong, T. Ohigashi, N. Kosugi, J. Wang, J. Zhou, T. Regierg, T. K. Shamh, Nanoscale 6 (2014) 9166–9176, http://dx.doi.org/10.1039/C4NR01961J.
[8] A.L. Ankudinov, B. Ravel, J.J. Rehr, S.D. Conradson, Phys. Rev. B 56 (1997) R1712.
[9] E.D. Crozier, J.J. Rehr, R. Ingalls, Amorphous and liquid systems, in: D. C. Konningsberger, R. Prins (Eds.), X-Ray Absorption: Principles, Applications and Techniques of EXAFS, SEXAFS and XANES, John Wiley & Sons, 1988, pp. 375–384.
[10] S. Yildirimcan, K. Ocakoglu, S. Erat, F.M. Emen, S. Repp, E. Erdem, Infrared and EPR spectroscopy, RSC Adv. 6 (2016) 39511–39521, http://dx.doi.org/10.1039/C6RA04071C.
[11] M.J. Akhtar, M. Ahamed, S. Kumar, M.M. Khan, J. Ahmad, S.A. Alrokayan, Int. J. Nanomed. 7 (2012) 845–857.
[12] I.A. Kowalik, G. Öhrwall, B.N. Jensen, R. Sankari, E. Wallen, U. Johansson, O. Karis, D. Arvanitis, J. Phys.: Conf. Ser. 211 (2010) 012030.
[13] W. Klysubun, et al., Commission and performance of x-ray absorption beamline at the Siam Photon Laboratory, Nucl. Instrum. Methods Phys. Res. A 582 (2007) 87–89.
[14] W. Klysubun, et al., X-ray absorption spectroscopy beamline at the Siam Photon Laboratory, AIP Conf. Proc. 879 (2006) 860–863.
[15] B. Ravel, J. Synchrotron. Radiat. 8 (2) (2001) 314.
[16] R.W.G. Wyckoff, 1st ed.,Crystal Structures, vol. 3, Interscience Publishers, New York, 1960.
[17] A.A. Mosquera, et al., Sci. Rep. 3 (2013) 1714, http://dx.doi.org/10.1038/srep01714.
[18] B. Ravel, M. Newville, J. Synchrotron. Radiat. 12 (4) (2005) 537.